

DOI:10.1002/ejic.201402708

## Mechanism of Nitric Acid Reduction and Kinetic Modelling

David Sicsic,<sup>[a]</sup> Fanny Balbaud-Célrier,<sup>\*[b]</sup> and Bernard Tribollet<sup>[c]</sup>

**Keywords:** Autocatalysis / Nitric acid / Nitrogen oxides / Reduction / Reaction mechanisms / Kinetics / Corrosion

In France, the recycling of nuclear waste fuels involves the use of hot concentrated nitric acid. The understanding and prediction of the behaviour of the structural materials (mainly austenitic stainless steels) requires the determination and modelling of the nitric acid reduction process. Nitric acid is indirectly reduced by an autocatalytic mechanism depending on the cathodic overpotential and acid concentration. This mechanism has been widely studied. All the authors agree on its autocatalytic nature, characterized by the predominant role of the reduction products. It is also generally admitted that neither nitric acid nor the nitrate ion is the electroactive species. However, the nature of the electroactive species, the place where the catalytic species regenerates and the thermodynamic and kinetic behaviour of the reaction intermediates remain uncertain. The aim of this study was to clarify some of these uncertainties by performing an electrochemical investigation of the reduction of 4 M nitric acid at 40 °C at an inert electrode (platinum or gold). An inert electrode was chosen as the working electrode in a first step to avoid its oxidation and focus the re-

search on the reduction mechanism. This experimental work enabled us to suggest a coherent sequence of electrochemical and chemical reactions. Kinetic modelling of this sequence was then carried out for a gold rotating disk electrode. A thermodynamic study at 25 °C allowed the composition of the liquid and gaseous phases of nitric acid solutions in the concentration range 0.5–22 M to be evaluated. The kinetics of the reduction of 4 M nitric acid was investigated by cyclic voltammetry and chronoamperometry at an inert electrode at 40 °C. The coupling of chronoamperometry and FTIR spectroscopy in the gaseous phase led to the identification of the gaseous reduction products as a function of the cathodic overpotential. The results showed that the reduction process is autocatalytic for potentials between 0.6 and 1.15 V/NHE. The electroactive species may be regenerated at the surface of the electrode for lower potentials, otherwise this regeneration process occurs in solution by a homogeneous chemical reaction. When the potential is less than 0.6 V/NHE, the fast reduction of nitrogen oxide may lead to rupture of the autocatalytic cycle.

### Introduction

In France, the recycling of waste fuel involves the use of nitric acid at various concentrations (up to the azeotropic concentration, 14.8 mol L<sup>-1</sup>) and temperatures up to their boiling point.<sup>[1]</sup> This specific medium can be corrosive towards structural materials, and for this reason highly corrosion-resistant materials have been selected. For the most severe conditions (high temperature and highly concentrated nitric acid), zirconium has been selected, and for other conditions stainless steels with very low carbon contents (the carbon level has to be below 0.03 wt.-%) are used, mainly AISI 304L stainless steel. However, in specific cases (condensation areas,<sup>[2]</sup> non-renewed media<sup>[3]</sup>), the autocatalytic mechanisms of the reduction of nitric acid may cause a shift of the steel's corrosion potential to the transpassive

domain leading to intergranular corrosion. Therefore, to understand, anticipate and predict the occurrence of such phenomena, a detailed comprehension and quantitative modelling of the nitric acid reduction mechanism are essential.

In a very general way, the behaviour of stainless steels in concentrated nitric acid can be schematized as shown in Figure 1.

Three anodic domains are observed as a function of the potential. At lower potentials, the active domain is observed; in this domain the steel undergoes homogeneous dissolution, which can lead to high corrosion rates (around several hundreds of μm per year). In this potential domain, the reduction process involves protons. At higher potentials, austenitic stainless steels such as 304L are in their passive domain, characterized by very low dissolution rates. Under these conditions, steels are protected by a very thin oxide layer (a few nm thick), mainly formed of chromium oxide (Cr<sub>2</sub>O<sub>3</sub>). In this domain, the reduction of nitric acid occurs.

The medium can be more oxidizing at higher nitric acid concentrations and temperatures or in the presence of oxidizing ions arising from fuel dissolution, for example, Pu<sup>VI</sup> or Np<sup>VI</sup>. In this last case, the reduction process is the re-

[a] CEA, DEN, DPC, SCCME, 91191 Gif-sur-Yvette, France

[b] CEA, DEN, DADN, 91191 Gif-sur-Yvette, France  
E-mail: fanny.balbaud@cea.fr  
<http://www.cea.fr/>

[c] Laboratoire Interfaces et Systèmes Electrochimiques, UPR15 du CNRS, Université Pierre et Marie Curie, 4 Place Jussieu, 75252 Paris Cedex 05, France

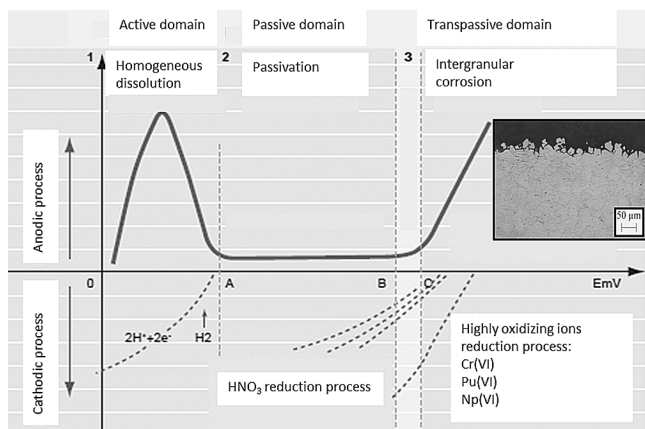


Figure 1. Schematic representation of the anodic and cathodic processes in nitric acid media.

duction of these oxidizing cations, otherwise it is the nitric acid reduction process. In this potential domain, called the transpassive domain, the steel undergoes intergranular corrosion.

One essential result of previous studies<sup>[2–5]</sup> was the demonstration of the crucial role of the nitric acid reduction process on the transition between the passive and transpassive domains and thus its impact on the corrosion process. Indeed, it has been shown that under some specific conditions, an increase in the concentration of the reduction products leads to an increase in the corrosion rate. This is the case in a confined and non-renewed medium (even for nitric acid concentrations at which the corrosion rate generally remains low) in which it was shown that increasing the concentration of nitric acid reduction products [nitrite ions were added that convert into nitrous acid ( $\text{HNO}_2$ ) in acidic medium] leads to a very important increase in the cathodic current and also to a very strong shift of the corrosion potential towards higher potentials reaching the lower end of the transpassive domain.<sup>[3]</sup>

Other measurements showed that in nitric acid condensates,<sup>[2]</sup> which are in fact similar to a confined and non-renewed medium (due to the very high metallic surface/solution volume ratio), a very strong influence of nitrogen monoxide flow on the corrosion of samples of 304L was observed.

Indeed, in the case of  $\text{N}_2$ ,  $\text{NO}_2$  and a 75% $\text{O}_2$ /25% $\text{N}_2$  mixture, there is no influence of the flow on the weight loss of the different specimens. However, a flow of nitrogen monoxide causes a sharp increase in the weight loss in the vapour phase and a high corrosion rate (for which severe intergranular corrosion occurs) is more quickly reached (after 15 days) than for the other gases or in the absence of a gas flow (after 35 days).

These two examples show the very strong influence of the reduction products (in these two cases,  $\text{HNO}_2$  and  $\text{NO}$ ) on the behaviour of materials in nitric acid under conditions of nitric acid concentration and temperatures at which the corrosion rate of 304L is usually low. This influence of the reduction products can appear a little contradictory as

one would assume that increasing the quantity of reduction products would decrease the corrosiveness of the medium. An understanding of the reduction process of nitric acid is thus essential and therefore identifying the species and the mechanisms involved and quantifying the reactions occurring is necessary. This will allow a better anticipation and prediction of potential corrosion concerns.

## Review of the Literature Data

The nitric acid reduction process has been widely studied over many years.<sup>[6–25]</sup> All through the 1950s and 1960s, two German teams supervised by Vetter and Schmid, respectively, made an important effort to determine the nitric acid reduction mechanism at platinum. Their studies of nitric acid solutions at concentrations of 1–10 mol L<sup>-1</sup> and containing nitrous acid at 25 °C led to different autocatalytic mechanisms.<sup>[7–14]</sup>

According to the literature, the nature of the reduction mechanism depends on two main parameters: the nitric acid concentration and the cathodic overpotential. The studies conducted at low concentrations of nitric acid ( $[\text{HNO}_3] < 1 \text{ mol L}^{-1}$ ) are not mentioned because in this case nitrates are directly reduced by a totally different mechanism.<sup>[23]</sup>

According to Vetter,<sup>[7–9]</sup> the mechanism is heterogeneous as the chemical regeneration of  $\text{NO}_2$ , assumed to be the electroactive species, occurs at the electrode surface.  $\text{NO}_2$  is formed at the interface according to a previous slow heterogeneous chemical reaction. In this case, the stirring of the solution has no influence on the current density. This mechanism can be described by reactions (1)–(5).



According to Schmid and co-workers, the mechanism is homogeneous, as the chemical regeneration of  $\text{NO}^+$ , assumed to be the electroactive species, occurs in the bulk.  $\text{NO}^+$  (equivalent to  $\text{HNO}_2$ ) is obtained from the nitrous acid formed in the layer near the electrode.<sup>[10–14]</sup> In this case, the stirring of the solution provokes a decrease in the current density. This mechanism can be described by reactions (6)–(10).



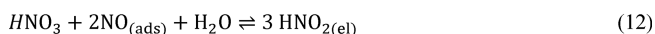
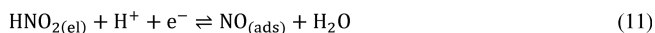
At the end of the 1980s, Razygraev et al. started new research into the behaviour of boiling 2 mol L<sup>-1</sup> nitric acid

solutions at a platinum electrode.<sup>[15]</sup> A voltammetric study was coupled to chemical, chromatographic and volumetric analysis of the reduction products. He concluded that the mechanisms of Vetter and Schmid occur successively at a platinum electrode according to the cathodic overpotential. Thus, Razygraev's observations at lower overpotentials ( $0.85 < E/SHE < 1.15$  V) may be characteristic of Vetter's mechanism, whereas at higher overpotentials ( $0.65 < E/SHE < 0.85$  V), Schmid's mechanism may occur.

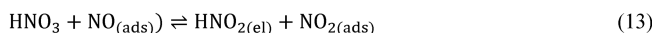
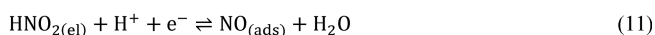
At potentials less than 0.65 V/SHE, the significant decrease in current density may be caused by the reduction of NO to N<sub>2</sub>O.

More recently, Balbaud et al. suggested a mechanism that is dependent upon the concentration of acid.<sup>[20]</sup> A thermodynamic study showed that the final product of the nitric acid reduction is NO for  $[HNO_3] < 6 \text{ mol L}^{-1}$  and NO<sub>2</sub> for  $[HNO_3] > 6 \text{ mol L}^{-1}$ .<sup>[26]</sup> A parallel electrochemical study was carried out at a platinum electrode in nitric acid solutions in the range 4–12 mol L<sup>-1</sup> at 100 °C, which showed that the charge-transfer step may be the reduction of HNO<sub>2</sub> to NO. The mechanism suggested is described by reactions (11)–(13). The subscript *el* indicates that the species is present in solution near the electrode.

- $[HNO_3] < 6 \text{ mol L}^{-1}$



- $[HNO_3] > 8 \text{ mol L}^{-1}$



These mechanisms are heterogeneous as the regeneration step takes place at the electrode. The gaseous species NO and NO<sub>2</sub> are adsorbed at the surface, and nitrous acid is a soluble compound formed at the electrode that diffuses into the solution.

Finally, in a recent study, Lange et al. proposed a mechanism in 8 M nitric acid solution at 20 °C to take into account solely the chemical steps that play a kinetic role.<sup>[25]</sup> They verified that the huge current enhancement (in the 0.95 to -0.45 V/SHE region) is due to autocatalysis and stems from the regeneration of HNO<sub>2</sub> in solution. A time- and potential-independent current plateau was observed for low scan rates, which was ascribed to a limitation resulting from the desorption of NO<sub>ads</sub>. They proposed the following mechanism based on the Schmid mechanism [reactions (14), (6) and (7)]



and the formation of HNO<sub>2</sub> through reactions (15) and (16).



The kinetic constants were determined by fitting of the experimental chronoamperograms and data analysis.

Finally, according to the literature, the reduction of concentrated nitric acid shows the following characteristics.

1) The mechanism is autocatalytic and the oxidation state of the nitrogenous regenerated species is III.

2) The reduction is indirect: neither nitric acid nor the nitrate ion is the electroactive species.

3) Beyond a certain cathodic overpotential, the production of N<sub>2</sub>O leads to a break in the catalytic cycle.

However, the complexity of the chemical reactions between nitrogenous species is responsible for discrepancies in the reduction mechanisms presented in the literature. In particular, the nature of the electroactive species and the place at which the regeneration step takes place are still poorly determined. In this work, our aim was to clarify some of these uncertainties, to identify the major species involved in the reduction of nitric acid, and to propose and establish a kinetic model for a sequence of reactions that explains the experimental observations.

## Results and Discussion

The electrochemical investigation was performed in a 4 mol L<sup>-1</sup> nitric acid solution at 40 °C. These conditions were chosen as they are intermediary conditions in the recycling process and because the reduction kinetics are not too fast under these conditions, thereby allowing an easier determination of the elementary steps.

Classical electrochemical techniques were used, namely cyclic voltammetry and chronoamperometry with a stationary electrode and a rotating disk electrode.

A typical cyclic voltammogram of a 4 mol L<sup>-1</sup> nitric acid solution with a Pt stationary electrode recorded at a sweep rate  $\nu = 20 \text{ mV s}^{-1}$  is represented in Figure 2. The electroactivity domain of nitric acid is limited by the reduction of protons ( $E = 0 \text{ V/SHE}$ ) and the oxidation of water ( $E = 1.6 \text{ V/SHE}$ ). Three potential ranges can be observed in the nitric acid reduction domain.

1)  $-0.9 \text{ V} < E/SHE < 1.15 \text{ V}$ : a first reduction wave is observed. The corresponding current densities are relatively low ( $< 1 \text{ mA cm}^{-2}$ ).

2)  $-0.6 \text{ V} < E/SHE < 0.9 \text{ V}$ : the cathodic current density strongly increases. This transition shows that a different reduction mechanism occurs during this second wave.

3)  $-0.4 \text{ V} < E/SHE < 0.6 \text{ V}$ : the marked decrease in the current density shows that the previous mechanism may be interrupted by another phenomenon.

This paper is focused on the second range of potentials. In this range, the sharp increase in the current density corresponds to the catalytic part of the reduction process, which is the interesting part with respect to the corrosion transition from a passive to a transpassive zone.

Figure 3 shows the results of a chronoamperometry test performed at a potential close to the beginning of the sec-

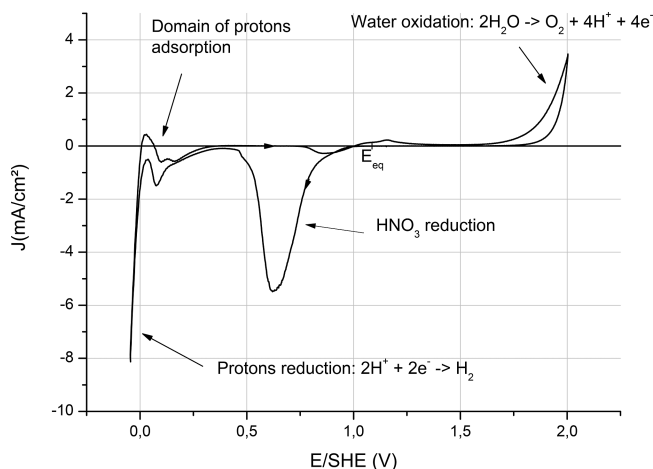


Figure 2. Cyclic voltammogram obtained at a stationary Pt electrode ( $4 \text{ mol L}^{-1} \text{ HNO}_3$ ,  $T = 40 \text{ }^\circ\text{C}$ ,  $v = 20 \text{ mV s}^{-1}$ ).

and cathodic wave ( $E = 0.9 \text{ V/SHE}$ ) at various rates of rotation of the rotating disk electrode after the addition of  $10^{-3} \text{ mol L}^{-1}$  of nitrites to fix the nitrite concentration during the test.

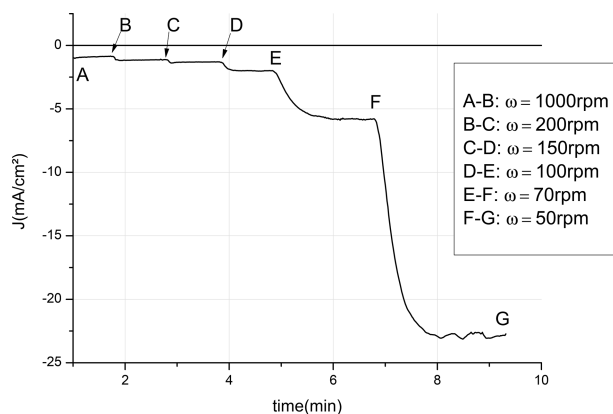


Figure 3. Influence of the rate of rotation of the current density during a chronoamperometry measurement ( $E = 0.9 \text{ V/SHE}$ , gold rotating disk,  $4 \text{ mol L}^{-1} \text{ HNO}_3 + 10^{-3} \text{ mol L}^{-1} \text{ NaNO}_2$ ,  $T = 40 \text{ }^\circ\text{C}$ ).

During this measurement the rate of disk rotation was changed from 1000 to 50 rpm. It is worth noting that, in general, the electroactive species diffuses from the solution towards the electrode and the limiting current is then proportional to  $\omega^{1/2}$  according to the Levich law.<sup>[27]</sup> In the present case it is clear that the current density does not follow the Levich law as its absolute value increases when the rate of rotation decreases. Only a few dozen rpm are sufficient to produce important variations of the current density, thus, the reduction process occurring in this potential range is partly controlled by the diffusion of the reactive species. The inverse effect of the rate of rotation shows that this species would not diffuse from the solution to the electrode, but that it would be generated close to or at the electrode. This species could be either the electroactive species or a reaction intermediate leading to the formation of the electroactive species by a chemical reaction. In both cases, by increasing the rate of rotation, this species would be chased

away from the electrode leading to the observed decrease in the current density.

These chronoamperometric measurements were repeated over a potential range from 1.05 to 0.7 V/SHE (corresponding to the end of the catalytic wave), and the variation in current densities versus potential are presented in Figure 4 for different rate of rotations of the disk. For each measurement, the stationary current was established 5–10 min after fixing the polarization potential and the rate of rotation of the disk.

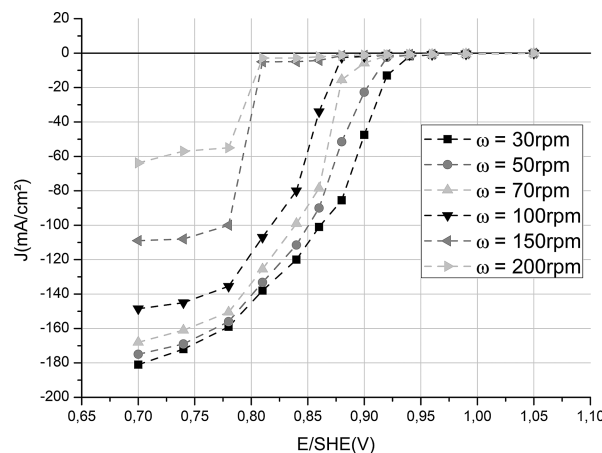


Figure 4. Steady-state current densities vs. potential and influence of the rate of rotation of a gold rotating disk ( $4 \text{ mol L}^{-1} \text{ HNO}_3 + 10^{-3} \text{ mol L}^{-1} \text{ NaNO}_2$ ,  $T = 40 \text{ }^\circ\text{C}$ ).

To check if a nitrogen(III) species is created near the electrode, samples of the solution were collected 1 mm from the platinum plate during the chronoamperometry measurement and analysed by the Griess method. The potential was fixed at 0.65 V/SHE, which corresponds to the catalytic wave. Table 1 presents the results of the analysis of nitrites during the test.

Table 1. Concentrations of the nitrogen(III) species during the chronoamperometry test presented in Figure 5.

$t$ [min]	$[\text{N}^{\text{III}}]$ [ $\text{mol L}^{-1}$ ]
0	$5.81 \times 10^{-6}$
8	$1.86 \times 10^{-4}$
9	$7.62 \times 10^{-5}$
20	$2.09 \times 10^{-4}$

The current densities and nitrogen(III) concentrations are presented in Figure 5 under the condition of stirring (+) or non-stirring (-). The results confirm that a dissolved  $\text{N}^{\text{III}}$  species may be the electroactive species and that it is regenerated close to the electrode by a chemical reaction as its concentration increases strongly when the solution is not stirred. We will assume that the major  $\text{N}^{\text{III}}$  species present in solution is nitrous acid ( $\text{HNO}_2$ ), but as was said previously,  $\text{NO}^+$  could also be considered an active species as it is always in equilibrium with  $\text{HNO}_2$  in acidic medium [reaction (5)]. In contrast, when the solution is stirred, this species is chased away from the electrode and so the catalytic cycle is disrupted and both the current density and the concentration of the nitrogen(III) species decrease.

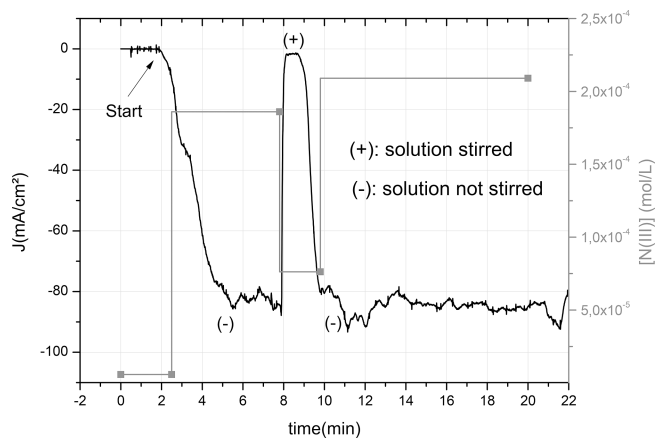


Figure 5. Measurements of nitrogen(III) during a chronoamperometry test at a Pt electrode ( $E = 0.65$  V/SHE,  $4 \text{ mol L}^{-1}$   $\text{HNO}_3$ ,  $T = 40$  °C).

Other chronoamperometry measurements were performed over the potential range of 0.05 to 1.05 V/SHE to study the evolution of the current density over 5000 s at different stages of the reduction process. The working electrode was a gold stationary plate and the medium ( $4 \text{ mol L}^{-1}$   $\text{HNO}_3$  at  $40$  °C) was renewed between each measurement. The current densities measured at different times as a function of potential are presented in Figure 6. The steady state was quickly obtained for potentials between 0.7 and 1.05 V/SHE. However, for lower potentials, the current densities increase until the end of the measurements. Although the catalytic cycle is supposed to be broken in this potential range, a new slow catalytic reduction process may occur. At the end of each test, a sample of the solution was collected to measure the concentration of nitrogen(III). The results are presented in Figure 7 as a function of potential. The concentrations obtained follow the variation in the current density. At the beginning of the reduction process, the concentration of nitrogen(III) is the same as that of a freshly made nitric acid solution, which means that  $\text{HNO}_2$

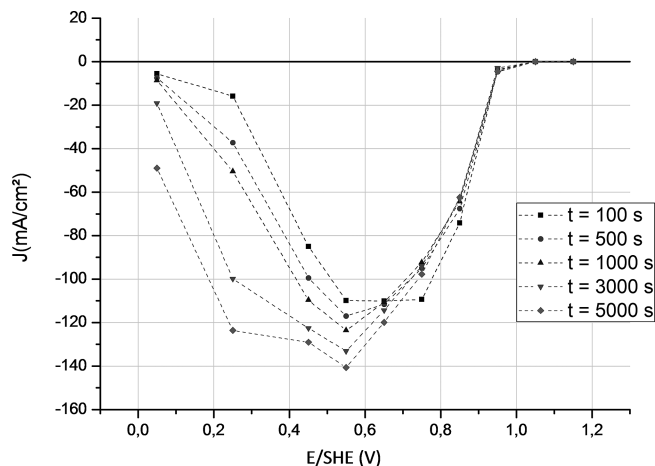


Figure 6. Voltammograms plotted from chronoamperometric measurements at a stationary gold electrode ( $4 \text{ mol L}^{-1}$   $\text{HNO}_3$ ,  $T = 40$  °C).

is not produced during the process or does not diffuse through the medium. During the catalytic wave, as expected, the concentration increases strongly and then drops because of a break in the catalytic cycle.

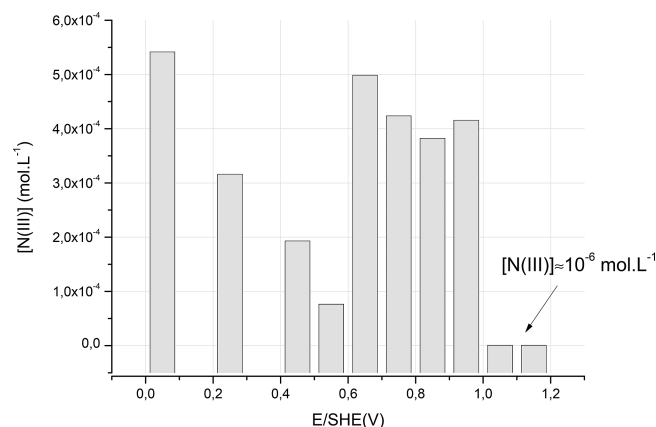


Figure 7. Concentration of nitrogen(III) in the solution at the end of the chronoamperometric measurements versus potential ( $4 \text{ mol L}^{-1}$   $\text{HNO}_3$ ,  $T = 40$  °C).

The gaseous reduction products were also analysed by FTIR spectroscopy. The spectra were recorded during chronoamperometric measurements of a  $4 \text{ mol L}^{-1}$  nitric acid solution in the potential range of 1.05 to 0.15 V/SHE. Different gases were detected depending on the potential imposed, thereby defining three potential domains.

Typical spectra corresponding to these domains are represented in Figure 8. From 1.05 to 1 V/SHE, absorption bands are observed at the vibrational frequencies of water ( $3756$ ,  $3657$  and  $1595 \text{ cm}^{-1}$ ) and carbon dioxide ( $2349 \text{ cm}^{-1}$ ).<sup>[28]</sup> These compounds are already present in the atmosphere above the nitric acid solution, which means that no gaseous reduction products are detected at these potentials. From 0.95 to 0.7 V/SHE, a band characteristic of NO ( $1880 \text{ cm}^{-1}$ ) can be observed in addition to the bands of water and carbon dioxide. NO is a very unstable species in the atmosphere of nitric media and is rapidly oxidized by

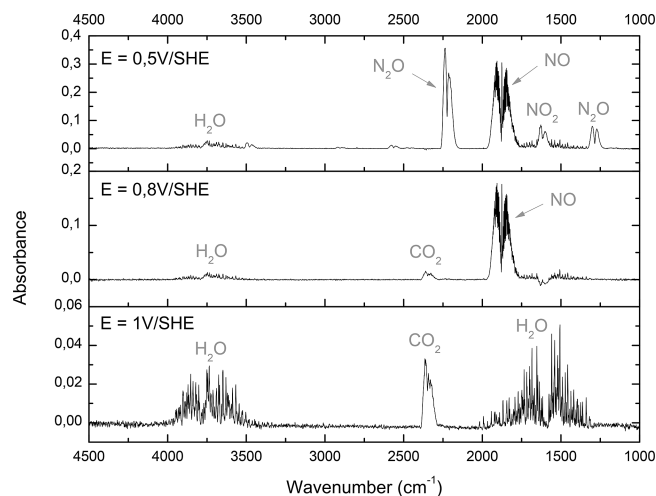


Figure 8. FTIR spectra of the reduction products in the gas phase at different potentials ( $4 \text{ mol L}^{-1}$   $\text{HNO}_3$ ,  $T = 40$  °C).

nitric acid or oxygen.<sup>[29]</sup> Therefore it cannot be produced by a chemical reaction in the gaseous phase, but must be the product of an electrochemical reaction. From 0.65 to 0.15 V/SHE, typical bands corresponding to N<sub>2</sub>O (2277 and 1300 cm<sup>-1</sup>)<sup>[28]</sup> and NO<sub>2</sub> (1610 cm<sup>-1</sup>)<sup>[28]</sup> are observed. These results confirm the hypothesis of Razygraev and co-workers that the break in the catalytic cycle is caused by the reduction of NO to N<sub>2</sub>O. Nevertheless, NO is still present in the gaseous phase, which means that these two mechanisms could be in competition in this potential range.

A spectrum of a 6 mol L<sup>-1</sup> nitric solution was recorded in the catalytic domain (Figure 9). A band corresponding to NO<sub>2</sub> is observed in addition to the band of NO, so at nitric acid concentrations greater than or equal to 6 mol L<sup>-1</sup>, this species could be a reduction product according to the mechanism described by Balbaud et al.<sup>[20]</sup>

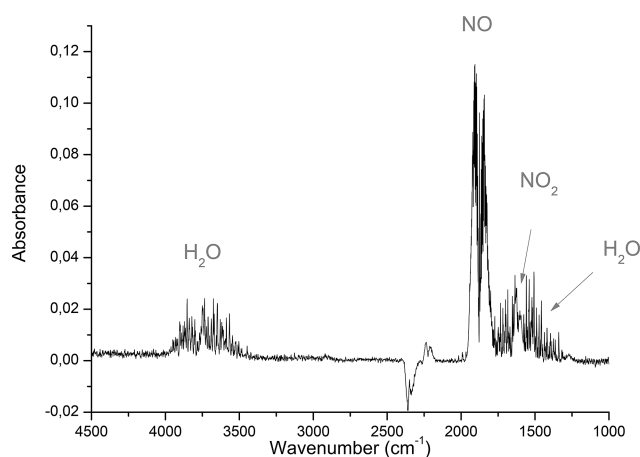


Figure 9. FTIR spectrum of the reduction products in the gas phase (6 mol L<sup>-1</sup> HNO<sub>3</sub>, *E* = 0.8 V/SHE, *T* = 40 °C).

Finally, to confirm the assignment of the different absorption bands to the species detected, pure water vapour and industrial preparations of NO, NO<sub>2</sub> and N<sub>2</sub>O dissolved in 100 ppm N<sub>2</sub> (Messer) were directly analysed in the FTIR gas cell. The spectra obtained for each gas are presented in

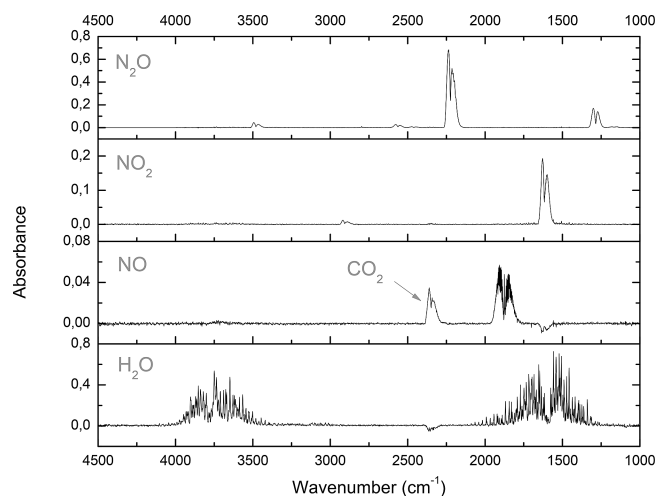
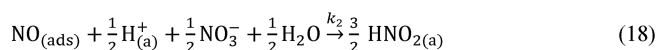
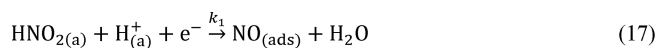


Figure 10. FTIR spectra of gaseous H<sub>2</sub>O, NO, NO<sub>2</sub> and N<sub>2</sub>O at ambient temperature.

Figure 10, and agree well with the literature data and the spectra described above. It would be interesting to quantify these analyses by calibrating the FTIR spectrometer for NO, NO<sub>2</sub> and N<sub>2</sub>O to access the kinetic constants.

### Reduction Mechanism and Kinetic Modelling

In the potential domain studied, the evolution of NO was detected and colorimetric titration measurements confirmed that HNO<sub>2</sub> is involved in the charge-transfer step and regenerated at or near the electrode by a chemical reaction. The act of stirring chases HNO<sub>2</sub> away from the electrode, which decreases the catalytic effect and the current densities. The mechanism considered for the modelling is similar to that of Balbaud et al.<sup>[20]</sup> at low HNO<sub>3</sub> concentrations and is described by reactions (17) and (18). The subscripted *a* indicates that the species is considered in its aqueous state.



There are three hypotheses that are important to consider in this mechanism.

1) NO is supposed to be an adsorbed intermediate at the electrode. The ability of NO to adsorb at inert electrodes in nitric media has already been suggested and validated in the literature by in situ FTIR measurements at inert electrodes.<sup>[22]</sup>

2) Reaction (18) is heterogeneous: HNO<sub>2</sub> regenerates at the electrode.

3) Both reactions are supposed to be irreversible. This hypothesis is reasonable as the cathodic overpotential is important and because the inverse kinetic constant of the homogeneous reaction corresponding to reaction (8) in solution is very low [the kinetic constants for the heterogeneous reaction (18) have not been found in the literature].

The desorption of adsorbed NO to gaseous NO should be included in the mechanism, but it will not be considered in the following modelling.

Having proposed a mechanism for the reduction of nitric acid at an inert electrode, the objective was then to develop a kinetic model for this mechanism. Comparison between the model and the experimental results at a gold rotating disk will enable support for the mechanism and eventually allow its modification. The approach adopted in this work deliberately set out to develop analytical modelling (as much as possible) to achieve a better mastering of the model in this first step of the modelling procedure.

Nitrous acid is supposed to diffuse from the electrode to the solution along the axis *y*. Thus, its concentration *C* is a solution of the convective-diffusion equation. Considering cylindrical coordinates, for reasons of symmetry and uniform accessibility of the disk, the angular and radial components of the equation can be neglected. When the steady-state current value is reached, the concentration near the electrode no longer varies and *dC/dt* = 0. These considera-

tions lead to a simplification of the convective-diffusion equation, which can be written as Equation (19).

$$v_y \left( \frac{dC}{dy} \right) = D \left( \frac{d^2C}{dy^2} \right) \quad (19)$$

in which  $D$  is the diffusion coefficient of  $\text{HNO}_2$  ( $\text{mol cm}^{-2}$ ) and  $v_y$  is the normal component of the fluid velocity profile given by Levich, see Equation (20).<sup>[27]</sup>

$$v_y = -0.51 \omega^{3/2} \nu^{-1/2} y^2 \quad (20)$$

in which  $\nu$  is the kinematic viscosity of the liquid ( $\text{cm}^2 \text{s}^{-1}$ ). Integration of Equation (19) leads to Equation (21).

$$C^* - C^0 = \left( \frac{dC}{dy} \right)_0 \int_0^\infty \exp \left( \frac{-0.17 \omega^{3/2} \nu^{-1/2}}{D} y^3 \right) dy \quad (21)$$

in which  $C^*$  and  $C^0$  are the concentrations of  $\text{HNO}_2$  in the bulk solution and at the electrode, respectively.

It is assumed that the concentration profile of  $\text{HNO}_2$  is linear and decreases across the diffusion layer of thickness  $\delta$ , see Equation (22).

$$C(y) = C^0 + (C^* - C^0)y/\delta \quad (22)$$

The analogy between the derivative for  $y = 0$  in Equation (22) and Equation (21) gives the thickness of the diffusion layer [Equation (23)].

$$\delta = 1.61 D^{1/3} \nu^{1/6} \omega^{-1/2} \quad (23)$$

The activities  $a(\text{H}^+)$ ,  $a(\text{NO}_3^-)$  and  $a(\text{H}_2\text{O})$  are supposed to be constant, so the apparent kinetic parameters  $k_1'$  and  $k_2'$  are introduced through Equations (24) and (25).

$$k_1' = k_1 a(\text{H}) \quad (24)$$

$$k_2' = k_2 [a(\text{H}^+) a(\text{NO}_3^-) a(\text{H}_2\text{O})]^{1/2} \quad (25)$$

The parameter  $k_1$  is the heterogeneous rate constant for reduction, and can be expressed by Equation (26).

$$k_1 = k_1^0 \exp \left( \frac{aF\eta}{RT} \right) \quad (26)$$

in which  $k_1^0$  is the standard electrochemical rate constant ( $\text{cm s}^{-1}$ ),  $a$  is the charge-transfer coefficient,  $F$  is the Faraday constant ( $\text{C mol}^{-1}$ ),  $R$  is the gas constant ( $\text{J mol}^{-1} \text{K}^{-1}$ ),  $T$  is the temperature (K),  $\eta$  is the cathodic overpotential (V), which is the difference between the electrode potential  $E$  (V/SHE) and the apparent normal potential  $E_0$ , which is equal to 1.09 V/SHE.

The two species with interfacial concentrations that impact on the reaction kinetics are NO and  $\text{HNO}_2$ . In the stationary regime, the surface coverage of  $\text{NO}_{(\text{ads})}$ ,  $\theta$ , is constant at the steady-state. Thus,  $\beta d\theta/dt = 0$ , which leads to Equation (27).

$$k_1' C^0 (1 - \theta) = k_2' \beta \theta \quad (27)$$

in which  $\beta$  ( $\text{mol cm}^{-2}$ ) is the maximum surface concentration of  $\text{NO}_{(\text{ads})}$ .

The flux of  $\text{HNO}_2$  at the surface of the disk can be written as Equation (28).

$$-D \left( \frac{dC}{dy} \right)_0 = \frac{3}{2} k_2' \beta \theta - k_1' C^0 (1 - \theta) \quad (28)$$

The cathodic steady-state current is proportional to the electrochemical reaction rate, given by Equation (29).

$$i_s = -FSk_1' C^0 (1 - \theta) \quad (29)$$

in which  $S$  is the disk area ( $\text{cm}^2$ ).

Combination of Equations (22), (27) and (28) leads to Equation (30).

$$-D \frac{(C^* - C^0)}{\delta} = \frac{1}{2} k_1' C^0 (1 - \theta) \quad (30)$$

An expression for the steady-state current is obtained by combining Equations (29) and (30) to give Equation (31).

$$i_s = 2DFS(C^* - C^0)/\delta \quad (31)$$

Moreover,  $C^0$  can be expressed as a function of the stationary current and the kinetic parameters according to Equation (32).

$$C^0 = \frac{-k_2' \beta i_s}{k_1' i_s + FSK_1' k_2' \beta} \quad (32)$$

By inserting Equation (32) into (31), an expression for  $\delta$  is obtained, see (33).

$$\delta = \frac{2DFSC^*}{i_s} + \frac{2DFSK_2' \beta}{k_1' i_s + FSK_1' k_2' \beta} \quad (33)$$

Equations (23) and (33) can then be combined to give a relationship between the rate of rotation and the stationary current, see Equation (34).

$$\omega^{-1/2} = \frac{A}{i_s} + \frac{B}{C + i_s} \quad (34)$$

With:

$$A = 1.242 FSD^{2/3} \nu^{-1/6} C^*$$

$$B = 1.242 FSD^{2/3} \nu^{-1/6} \beta (k_2'/k_1')$$

$$C = FSK_2' \beta$$

The representation of  $\omega^{-1/2}$  as a function of the stationary current measured experimentally allows the determination of  $A$ ,  $B$  and  $C$ , and then the adjustment of  $k_1'$  and  $k_2'$ , which have not been found in the literature.

Finally, the expression of the stationary current as a function of potential (implicitly expressed in  $k_1'$ ) and the rate of rotation of the disk (implicitly expressed in  $\delta$ ) is given by the negative solution of Equation (33), that is, (35).

$$i_s = \frac{1}{2k_1' \delta} \left\{ FSC(2C^* Dk_1' + 2\beta Dk_2' - \beta k_1' k_2' \delta) - \sqrt{8F^2 S^2 \beta C^* Dk_1'^2 k_2' \delta + [FS(\beta k_1' k_2' \delta - 2C^* Dk_1' - 2\beta Dk_2')]^2} \right\} \quad (35)$$

The parameters used in the model are given in Table 2.

Table 2. Values of input data for the heterogeneous model.

Model parameter	Value
$F$ [C mol <sup>-1</sup> ]	96485
$R$ [J mol <sup>-1</sup> K <sup>-1</sup> ]	8.314
$T$ [K]	313 <sup>[a]</sup>
$S$ [cm <sup>2</sup> ]	0.196 <sup>[a]</sup>
$\nu$ [cm <sup>2</sup> s <sup>-1</sup> ]	$7.4 \times 10^{-3}$ <sup>[b]</sup>
$a$	0.5 <sup>[c]</sup>
$\beta$ [mol cm <sup>-2</sup> ]	$2 \times 10^{-9}$ <sup>[d]</sup>
$C^*$ [mol cm <sup>-3</sup> ]	$10^{-6}$ <sup>[a]</sup>
$a(\text{H}^+) = a(\text{NO}_3^-)$	$5.27 \times 10^{-3}$ <sup>[e]</sup>
$a(\text{H}_2\text{O})$	0.816 <sup>[e]</sup>

[a] Measured. [b] See ref.<sup>[30]</sup> [c] Adjusted. [d] See ref.<sup>[31]</sup> [e] See ref.<sup>[32]</sup>

The results obtained from the chronoamperometry tests at the rotating disk (Figure 4) were fitted to Equation (34) at different potentials to obtain values of  $A$ ,  $B$  and  $C$ . The mean values of these parameters are as follows:  $A = 3.43 \times 10^{-5} \text{ A s}^{1/2}$ ,  $B = 1.48 \times 10^{-2} \text{ A s}^{1/2}$  and  $C = 3.52 \times 10^{-5} \text{ A}$ .

By using  $A$ ,  $B$  and  $C$  it is possible to determine  $k_1'$ ,  $k_2'$  and the diffusion coefficient of  $\text{HNO}_2$ ,  $D$ . Then, by using Equation (24),  $k_1$  can be determined, and finally, the standard electrochemical rate constant  $k_1^0$  can be determined by using Equation (26). The diffusion layer thickness,  $\delta$ , can also be calculated (numerical application for  $\omega = 100 \text{ rpm}$ ). The following values were obtained:  $D = (1.81 \pm 0.56) \times 10^{-5} \text{ cm}^2 \text{ s}^{-1}$ ,  $k_1^0 = 0.02 \pm 0.01 \text{ cm s}^{-1}$ ,  $k_2' = 900 \pm 600 \text{ s}^{-1}$  and  $\delta = 60 \mu\text{m}$ .

The diffusion coefficient of  $\text{HNO}_2$ ,  $D$ , at  $40^\circ \text{C}$  is missing from the literature, but the value obtained in this study is in accordance with measurements in a  $4 \text{ mol L}^{-1}$  nitric acid solution at  $100^\circ \text{C}$ :<sup>[20]</sup>  $8 \times 10^{-6} < D < 9 \times 10^{-5} \text{ cm}^2 \text{ s}^{-1}$ .

Finally, having defined and evaluated all the parameters, it is possible to calculate the theoretical stationary current density as a function of the overpotential. These plots and experimental data from Figure 4 are represented in Figure 11 for four different rates of rotation.

At low overpotentials, the kinetic parameter  $k_1$  is low, so the electrochemical reaction is slow compared with the chemical reaction, and the current densities remain relatively low. Thus, the kinetics of the reduction process is limited by the rate of the charge-transfer step. For higher overpotentials, the current density of the plateau is determined by the value of  $k_2$ , so the kinetics of the process are limited by the rate of the catalytic chemical reaction. This value does not depend on the rate of rotation of the disk, as shown by Equation (28) for high overpotentials: in this case, the term  $B/(C + i_s)$  tends towards zero. Between these two domains, the kinetics is controlled by the rates of both the chemical and electrochemical steps and by the diffusion of  $\text{HNO}_2$ .

At low values of  $\omega$  (30 to 70 rpm), the model fits well with the experimental points. In particular, the sudden increase in the current density and the surprising influence of the rate of rotation are well described. However, at higher values of  $\omega$  ( $\geq 100 \text{ rpm}$ ) and overpotentials, the experimental current densities of the plateau are lower than those ex-

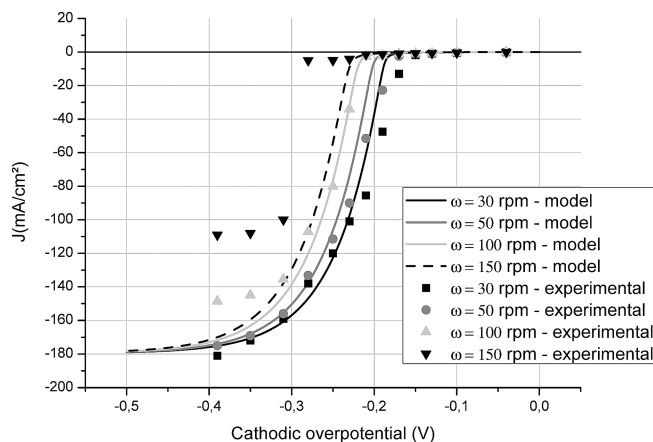
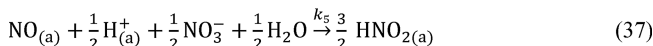
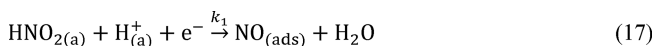


Figure 11. Variation of the stationary current density as a function of the cathodic overpotential. Comparison of the model presented in Equation (35) with the experimental results obtained at a gold rotating disk electrode ( $4 \text{ mol L}^{-1} \text{ HNO}_3 + 10^{-3} \text{ mol L}^{-1} \text{ NaNO}_2$ ,  $T = 40^\circ \text{C}$ ).

pected by the model. This difference can be explained by the fact that under these conditions, the heterogeneous mechanism proposed herein would not represent the global process. In fact, the chemical reaction allowing the regeneration of  $\text{HNO}_2$  may not occur only at the surface of the electrode as considered here, but in the solution close to the electrode. Indeed, the intermediate  $\text{NO}$  quickly and abundantly formed at the electrode would diffuse into solution and the homogeneous regeneration reaction would be predominant.

In that case, the mechanism of reduction would be given by reactions (17), (36) and (37).



As in the previous modelling of a heterogeneous mechanism, the system is considered to be stationary and the concentrations of  $\text{NO}$  and  $\text{HNO}_2$  are assumed to be independent of the radius,  $r$ , and the angle,  $\phi$ , of the cylindrical coordinates.

By considering  $C_1 = [\text{HNO}_{2(a)}]$  and  $C_2 = [\text{NO}_{(a)}]$ , the convective-diffusion equations have to be modified because at a given point of the solution,  $\text{HNO}_{2(a)}$  is produced and  $\text{NO}_{(a)}$  is consumed according to reaction (37). According to the literature,<sup>[33]</sup> this reaction would itself be the result of a more complex catalytic process. The kinetics of this process would be first order in  $\text{HNO}_2$  and zero order in  $\text{NO}$ . To simplify the resolution, only reaction (37) will be considered and it will be assumed to be zero order in  $\text{NO}$ .

The rate of production of  $\text{HNO}_2$  by the chemical reaction is thus given by Equation (38).

$$\left(\frac{dC_1}{dt}\right) = \frac{3}{2} k_5 C_1 \quad (38)$$

in which  $k_5' = k_5[a(\text{H}^+)a(\text{NO}_3^-)a(\text{H}_2\text{O})]^{1/2}$ .

The consumption of NO by the chemical reaction is described by Equation (39).

$$\left(\frac{dC_2}{dt}\right) = -k_5' \quad (39)$$

The convective-diffusion equations for NO and HNO<sub>2</sub> can thus be described by Equation (40).

$$\begin{cases} v_y \left(\frac{dC_1}{dy}\right) = D_1 \left(\frac{d^2C_1}{dy^2}\right) + \frac{3}{2}k_5' \\ v_y \left(\frac{dC_2}{dy}\right) = D_2 \left(\frac{d^2C_2}{dy^2}\right) - k_5' \end{cases} \quad (40)$$

in which  $D_1$  and  $D_2$  are diffusion coefficients of HNO<sub>2</sub> and NO (cm<sup>2</sup>s<sup>-1</sup>) and  $v_y$  is the normal component of the fluid velocity given by Levich [Equation (20)].<sup>[27]</sup>

The concentration profiles  $C_1(y)$  and  $C_2(y)$  were calculated numerically by using the Mathematica software. This resolution requires four boundary conditions. In solution ( $y \rightarrow \infty$ ), the concentrations of HNO<sub>2</sub> and NO are constant, whatever the overpotential, see Equations (41) and (42).

$$C_1(\infty) = 10^{-6} \text{ mol cm}^{-3} \quad (41)$$

$$C_2(\infty) = K \quad (42)$$

$C_1(\infty)$  was measured experimentally. The resolution tests of this system showed that the current density is independent of  $K$ . However,  $K$  has to be fixed to a non-zero value to ensure the convergence of the calculation. The value of  $K$  was fixed to  $3 \times 10^{-4} \text{ mol cm}^{-3}$ , which allows the convergence of the calculations. The concentrations of HNO<sub>2</sub> and NO for  $y = 0$  at the stationary state ( $C_1^0$  and  $C_2^0$ , respectively) are not known, and thus the two other boundary conditions have to be determined from the expression of the flux of these species at the electrode surface, see Equations (43) and (44).

$$D_1 \left(\frac{dC_1}{dy}\right)_0 = k_1' C_1^0 (1 - \theta) \quad (43)$$

$$D_2 \left(\frac{dC_2}{dy}\right)_0 = k_4 \beta \theta \quad (44)$$

The desorption reaction of NO<sub>(ads)</sub> at the stationary state leads to Equation (45).

$$k_1' C_1^0 (1 - \theta_s) = k_4 \beta \theta_s \quad (45)$$

The stationary surface coverage of NO<sub>(ads)</sub> can thus be expressed by Equation (46).

$$\theta_s = \frac{k_1' C_1^0}{k_1' C_1^0 + k_4 \beta} \quad (46)$$

By combining Equations (43) and (46), the first boundary condition for  $y = 0$  is obtained, see Equation (47).

$$\left(\frac{dC_1}{dy}\right)_0 = \frac{k_1' k_4 \beta C_1^0}{D_1 (k_1' C_1^0 + k_4 \beta)} \quad (47)$$

The second boundary condition for  $y = 0$  is obtained from Equations (43), (44) and (45), see Equation (48).

$$D_1 \left(\frac{dC_1}{dy}\right)_0 + D_2 \left(\frac{dC_2}{dy}\right)_0 = 0 \quad (48)$$

Once the stationary concentration profiles  $C_1(y)$  and  $C_2(y)$  have been numerically determined, the stationary current density can be calculated according to Equation (49).

$$i_s = -FSD_1 \left(\frac{dC_1}{dy}\right)_0 \quad (49)$$

The input data of the model are the same as for the heterogeneous model previously described. The adjusted or calculated parameters have also been adjusted to the same values as in the heterogeneous model ( $a$ ,  $D_1 = D_2$ ; Table 3):

Table 3. Values of input data for the homogeneous model.

Model parameter	Value
$F$ [C mol <sup>-1</sup> ]	96485
$R$ [J mol <sup>-1</sup> K <sup>-1</sup> ]	8.314
$T$ [K]	313 <sup>[a]</sup>
$S$ [cm <sup>2</sup> ]	0.196 <sup>[a]</sup>
$v$ [cm <sup>2</sup> s <sup>-1</sup> ]	$7.4 \times 10^{-3}$ <sup>[b]</sup>
$a$	0.5 <sup>[c]</sup>
$\beta$ [mol cm <sup>-2</sup> ]	$2 \times 10^{-9}$ <sup>[d]</sup>
$C^*$ [mol cm <sup>-3</sup> ]	$10^{-6}$ <sup>[a]</sup>
$a(\text{H}^+) = a(\text{NO}_3^-)$	$5.27 \times 10^{-3}$ <sup>[e]</sup>
$a(\text{H}_2\text{O})$	0.816 <sup>[e]</sup>
$D_1 = D_2$ [cm <sup>2</sup> s <sup>-1</sup> ]	$1.81 \times 10^{-5}$ <sup>[f]</sup>
$k_0^1$ [cm s <sup>-1</sup> ]	0.02

[a] Measured. [b] See ref.<sup>[30]</sup> [c] Adjusted. [d] See ref.<sup>[31]</sup> [e] See ref.<sup>[32]</sup> [f] Calculated.

Finally, the kinetic constants of the chemical reactions were adjusted with the experimental values of the current density:  $k_4 = 900 \text{ s}^{-1}$  and  $k_5' = 1.86 \times 10^{-4} \text{ s}^{-1}$ .

Calculated values of  $i_s = f(\eta_c)$  according to Equation (49) together with experimental measurements of the stationary current density by chronoamperometry are presented in Figure 12 as a function of overpotential for two rates of rotation of the disk electrode.

For low overpotentials, the homogeneous model does not allow the variation of the current density to be represented,

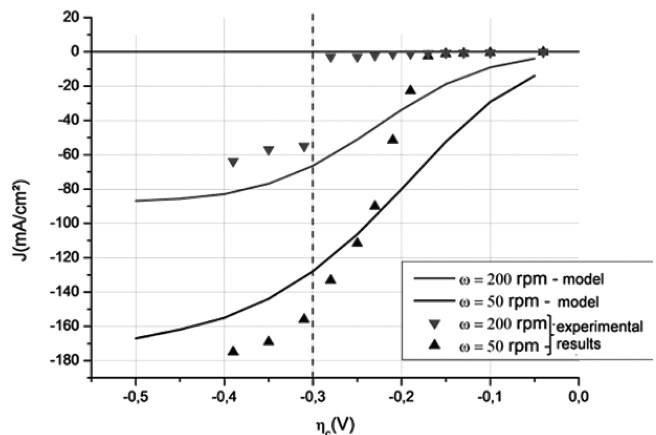


Figure 12. Variation of the stationary current density as a function of the cathodic overpotential. Comparison of the model Equation (44) with the experimental results obtained at a gold rotating disk electrode ( $4 \text{ mol L}^{-1} \text{ HNO}_3 + 10^{-3} \text{ mol L}^{-1} \text{ NaNO}_2$ ,  $T = 40 \text{ }^\circ\text{C}$ ).

whereas the heterogeneous model is well adapted. The chemical regeneration of  $\text{HNO}_2$  would therefore occur at the electrode surface. However, for higher overpotentials, ( $|\eta_c| > 0.3 \text{ V}$ ), the homogeneous model represents the current density well, contrary to the heterogeneous model, which predicts a constant value for the current density (see Figure 11) whatever the rate of rotation of the disk, this value being far from the experimental values for  $\omega \geq 100 \text{ rpm}$ . Under these conditions of high overpotential ( $|\eta_c| > 0.3 \text{ V}$ ) and rates of rotation ( $\omega \geq 100 \text{ rpm}$ ), the nitrogen monoxide formed by the electrochemical reaction in high quantities would be chased away from the electrode by convection to react in the homogeneous phase with nitric acid to regenerate nitrous acid.

## Conclusions

To gain a better understanding of corrosion mechanisms of stainless steels in concentrated nitric acid and to develop a predictive and quantitative approach to these phenomena, a model of the nitric acid reduction process has been developed. In a first approach, only measurements at an inert electrode (platinum or gold) were taken to focus on the reduction process. In agreement with the literature data, the catalytic nature of the reduction process was evidenced and a mechanism was proposed for the catalytic part of the global reduction mechanism. The results suggest that  $\text{HNO}_2$  is the electroactive species and that it is regenerated at or near the electrode surface by a chemical reaction between  $\text{HNO}_3$  and  $\text{NO}_{(\text{ads})}$ . In particular, stirring has an unusual and significant effect as it chases away  $\text{HNO}_2$  from the electrode and slows down the kinetics of the process. A two-step mechanism involving an electrochemical and chemical reaction, both heterogeneous and irreversible, was suggested. The kinetic modelling of this mechanism carried out for a rotating disk system fits well with the experimental data at low rates of rotation. The potential of the transition between the two kinetic regimes is shifted towards higher overvoltages when  $\omega$  is increased. However, when  $\omega$  is greater than 100 rpm, the limiting current density of the plateau is not well described by the model. Indeed, for these conditions, the kinetic model including the regeneration of  $\text{HNO}_2$  in solution and not at the electrode allows a good description of the experimental results. However, these are the first calculations and they need to be consolidated, for example, specific experimental work could be performed to determine the kinetic constants that were adjusted from these calculations.

Finally, considering the applicability of this work to austenitic stainless steel 304L, electrochemical tests (cyclic voltammetry and chronoamperometry) were performed at a stainless-steel electrode to confirm the proposed mechanism.<sup>[2]</sup> These electrochemical measurements were carried out in  $4 \text{ mol L}^{-1} \text{ HNO}_3$  at  $100 \text{ }^\circ\text{C}$ .<sup>[2]</sup> The results obtained showed that the reduction process is much slower at the stainless-steel electrode than at the platinum electrode at the same temperature. Indeed, it was necessary to impose much

higher overvoltages on the stainless-steel electrode than on the platinum electrode to obtain comparable current densities. Chronoamperometric measurements were performed to study the effect of stirring of the electrode. The rotation of the electrode led to a sharp decrease (in magnitude) of the current density, which shows that the electroactive species is not nitric acid. Moreover, a series of experiments were performed in nitric acid solutions containing nitrous acid at a concentration close to  $10^{-2} \text{ mol L}^{-1}$ . In these experiments, the corrosion potential was shifted towards high potentials. Moreover, in the presence of nitrites, the current densities in oxidation as well as in reduction were higher (as has already been observed for platinum<sup>[20]</sup>). This increase shows that nitrous acid promotes the reduction of nitric acid on stainless steel.

As the chronoamperometric measurements showed that nitric acid was not the electroactive species, and that it was a soluble species formed at the electrode that diffuses through solution, it was possible to assume that, as at platinum, nitrous acid is the electroactive species.

Finally, it is possible to assume that the reduction mechanism is identical at both electrodes except that it proceeds at a much lower rate at the 304L stainless-steel electrode. Of course, it is now necessary to verify that the modelling established for platinum in this paper would be the same in the case of stainless steel.

## Experimental Section

**General:** Classical electrochemical techniques were used: cyclic voltammetry and chronoamperometry with a stationary electrode and a rotating disk electrode.

Electrochemical experiments were conducted at  $40 \text{ }^\circ\text{C}$  in a reactor containing  $4 \text{ mol L}^{-1}$  nitric acid (200 mL). The gas volume above the reactor was also 200 mL. The stationary working electrodes consisted of a platinum plate (area  $0.5 \text{ cm}^2$ ) or a gold plate (area  $2 \text{ cm}^2$ ). A Radiometer EDI-101 gold rotating disk (diameter 5 mm) was used to study the hydrodynamic effects of the reduction process.

In very acidic and corrosive media, such as concentrated nitric acid, an oxide layer  $\text{PtO}_2$  may form on the platinum.<sup>[34]</sup> Indeed, the open circuit potential of an inert electrode in a  $4 \text{ mol L}^{-1}$  nitric acid solution at  $40 \text{ }^\circ\text{C}$  is about 1.15 V/SHE. At this acidity, platinum can be oxidized at potentials above 1 V/SHE and gold for potentials above 1.3 V/SHE. Thus, it is preferable to use gold as the working electrode material in these media to avoid the reduction of  $\text{PtO}_2$  during electrochemical measurement.

The working electrode was treated electrochemically before each test to clean it and then afterwards to remove the eventual adsorbed species at its surface. This treatment consisted of imposing a potential of  $-0.5 \text{ V/SHE}$  at the electrode so that bubbles of hydrogen produced in the reduction of water can clean it. Thus, the condition of the surface of the electrode is the same for each measurement.

The counter electrode was a platinum wire and the reference electrode was a mercurous sulfate electrode (SSE) separated from the nitric media by a salt bridge filled with a saturated  $\text{KNO}_3$  solution. The potential of this reference electrode versus the standard

hydrogen electrode (SHE) at 25 °C was  $E_{SSE} = 0.65$  V/SHE.<sup>[34]</sup> All the measurements were made with a Bio-logic VSP potentiostat.

The influence of nitrous acid was studied by adding sodium nitrite  $\text{NaNO}_2$  in the solution. The quantity of nitrogen(III) ( $\text{HNO}_2$  or  $\text{NO}^+$ ) in the solution was measured by UV/Vis spectroscopy with a Varian Carry 50 spectrophotometer according to the Griess method.<sup>[35]</sup>

Chronoamperometry was coupled with gas IR spectroscopy to analyse the reduction products in the gaseous phase as a function of the electrode cathodic overpotential. A Varian Excalibur 3100 FTIR spectrophotometer fitted with a multiple reflections gas cell (volume 2.5 L) was used. The number of laser reflections in the cell could be adjusted to obtain the desired optical path length, which was set to 2 m in our experiments. A long optical path length is in fact necessary to detect the small quantities of gas generated during the reduction process.

Nitrogen (purity 4.5) was used as the carrier gas (flow rate  $5 \text{ L h}^{-1}$ ). The nitric vapours created in the electrochemical cell were dried in a silica gel column to limit the presence of water, which is a highly absorbing species in IR spectroscopy. Then the vapours were analysed in the FTIR gas cell heated at 80 °C to avoid condensation and finally destroyed in a  $1 \text{ mol L}^{-1}$  sodium hydroxide solution. All the spectrograms were recorded at a resolution of  $2 \text{ cm}^{-1}$  in a wavenumber range between 400 and  $5000 \text{ cm}^{-1}$ .

## Acknowledgments

The authors want to thank Areva NC for financial support. They also want to thank P. Fauvet and N. Gruet from CEA for their interest in this work and fruitful scientific discussions.

- [1] Monographie DEN, *Le Traitement Recyclage du Combustible Nucléaire Usé* (Ed.: B. Bonin), Editions CEA/Saclay et Groupe Moniteur, Paris, **2008**, p. 33–36.
- [2] F. Balbaud, G. Sanchez, P. Fauvet, G. Santarini, G. Picard, *Corros. Sci.* **2000**, *42*, 1685–1707.
- [3] J. P. Schosger, F. Dabosi, R. Demay, P. Fauvet, J. P. Moulin, G. Santarini, *Influence of corrosion products on the passivation of AISI 304L stainless steel, in: nitric acid media*, in: *Proceedings of EUROCORR 96 Conference*, Nice, September 24–26, **1996**.
- [4] P. Fauvet, F. Balbaud-Célérier, R. Robin, Q.-T. Tran, A. Mugnier, D. Espinoux, *J. Nucl. Mater.* **2008**, *375*, 52–64.
- [5] R. Robin, F. Balbaud, P. Fauvet, N. Gruet, B. Gwinner, *Corrosion Issues about the Materials of the French Fuel Reprocessing*, in: *Proceedings of GLOBAL 2011*, Makuhari, Japan, December 11–16, **2011**.
- [6] W. J. Plieth, in: *Encyclopedia of Electrochemistry of the Elements* (Ed.: A. J. Bard), Marcel Dekker, New York, **1978**, vol. 8, p. 321.
- [7] K. Vetter, *Z. Phys. Chem. (Leipzig)* **1950**, *194*, 199–206.
- [8] K. Vetter, *Z. Phys. Chem. (Leipzig)* **1950**, *194*, 284–296.
- [9] K. Vetter, *Z. Elektrochem. Ber. Bunsenges. Physik. Chem.* **1959**, *63*, 1189–1191.
- [10] G. Schmid, *Z. Elektrochem. Ber. Bunsenges. Physik. Chem.* **1959**, *63*, 1183–1188.
- [11] G. Schmid, J. Delfs, *Z. Elektrochem. Ber. Bunsenges. Physik. Chem.* **1959**, *63*, 1192–1197.
- [12] G. Schmid, *Z. Elektrochem. Ber. Bunsenges. Physik. Chem.* **1961**, *65*, 531–534.
- [13] G. Schmid, G. Krichel, *Z. Elektrochem. Ber. Bunsenges. Physik. Chem.* **1964**, *68*, 677–688.
- [14] G. Schmid, M. A. Lobeck, *Z. Elektrochem. Ber. Bunsenges. Physik. Chem.* **1969**, *73*, 89–199.
- [15] V. P. Razygraev, M. V. Lebedeva, S. A. Kabakchi, E. Y. Ponomareva, R. S. Balovneva, L. P. Lobanova, *Zh. Prikl. Khim.* **1988**, *61*, 71–79.
- [16] V. P. Razygraev, R. S. Balovneva, E. Yu. Ponomareva, M. V. Lebedeva, *Zashch. Met.* **1990**, *26*, 54–60.
- [17] J. Masek, *Polarographic behaviour of nitrate and nitrite ions in strongly acidic media*, in: *Advances in Polarography*, 2nd International Congress, Cambridge, UK, **1959**.
- [18] E. N. Mirolyubov, *Zh. Prikl. Khim.* **1962**, *35*, 132–138.
- [19] M. Lemaire, *Optimisation des conditions opératoires de production de vapeurs nitreuses par réduction électrochimique d'acide nitrique*, Ph.D. Thesis, Université Paul Sabatier, Toulouse, France, **1996**.
- [20] F. Balbaud, G. Sanchez, G. Santarini, G. Picard, *Eur. J. Inorg. Chem.* **2000**, 665–674.
- [21] O. W. J. S. Rutten, A. Van Sandwijk, G. Van Weert, *J. Appl. Electrochem.* **1999**, *29*, 87–92.
- [22] M. C. P. M. Da Cunha, J. P. I. De Souza, F. C. Nart, *Langmuir* **2000**, *16*, 771–777.
- [23] M. T. De Groot, M. T. M. Koper, *J. Electroanal. Chem.* **2004**, *562*, 81–94.
- [24] R. D. Armstrong, G. E. Cleland, G. O. H. Whillock, *J. Appl. Electrochem.* **1998**, *28*, 1205–1211.
- [25] R. Lange, E. Maisonhaute, R. Robin, V. Vivier, *Electrochem. Commun.* **2013**, *29*, 25–28.
- [26] F. Balbaud, G. Sanchez, G. Santarini, G. Picard, *Eur. J. Inorg. Chem.* **1999**, *2*, 277–285.
- [27] V. G. Levich, in: *Physicochemical Hydrodynamics*, Prentice-Hall, Englewood Cliffs, NJ, **1962**.
- [28] K. Nakamoto, *Infrared and Raman Spectra of Inorganic and Coordination Compounds*, Part A, Wiley, **2009**.
- [29] J. B. Joshi, V. V. Mahajani, V. A. Juvekar, *Chem. Eng. Commun.* **1985**, *33*, 1–92.
- [30] P. Pascal, *Nouveau Traité de Chimie Minérale*, Masson, Paris, **1956**, vol. 10.
- [31] A. J. Bard, L. R. Faulkner, *Electrochimie: principes et applications*, Masson, Paris, **1983**.
- [32] W. Davis, H. J. De Bruin, *J. Inorg. Nucl. Chem.* **1964**, *26*, 1069–1083.
- [33] G. Carta, R. L. Pigford, *Ind. Eng. Chem. Fundamentals* **1983**, *22*, 329–335.
- [34] M. Pourbaix, *Atlas d'équilibres électrochimiques*, Gauthier-Villars & Cie, Paris, **1963**.
- [35] J. Sun, X. Zhang, M. Broderick, H. Fein, *Sensors* **2003**, *3*, 276–284.

Received: July 25, 2014

Published Online: November 25, 2014